Preliminary Report: On the feasibilty of a Passive Doppler Precipitation Radar (PDPR) to measure rainfall and windspeed from the scatter of broadcast signals transmitted by geostationary communication satellites

J. W. Diamond, S. Hawk, J. D. Sahr*
Department of Electrical Engineering, University of Washington
Seattle WA 98195-2500
J. Weinman
‘ *Microwave Sensors Branch, Code 975*
NASA Goddard Space Flight Center
Greenbelt MD 20771

December 18, 2002

Abstract

This report[1] provides a preliminary analysis of a passive Doppler radar system to remotely sense precipitation and windspeed by observing the scatter of microwave broadcasts from geosynchronous satellites. Completely passive radar systems have begun to appear for aerospace and ionospheric applications (observing terrestrial VHF and UHF transmissions), successfully demonstrating the principle of passive radars. Thus we consider the exploitation of microwave broadcasts at frequencies similar to conventional precipitation radars. This report describes a link budget analysis for a candidate radar system and describes a simpler “proof of concept” instrument that could be developed fairly easily before committing to a more elaborate instrument.

We conclude that it is unlikely to be able to build a completely passive system with space-time resolution that meets the needs of the weather community with currently available transmitters. Should anticipated more powerful

*diamond@ee.washington.edu, jdsahr@u.washington.edu
[1]funding provided by NASA, grant NAG5-11372

sources become available, the PDPR with lower procurement cost and much lower operation cost, would be very welcome.

1 Introduction

In this report we provide a preliminary examination of the engineering requirements for estimating rainfall and windspeed distributions from ground-based observation of the scatter of broadcast signals transmitted from geostationary satellites. This work will directly suggest development of a ground-based "proof of concept" instrument with limited capacity. Successful demonstration would justify a more fully fledged ground-based weather radar system.

1.1 Precipitation and Wind Shear Measurements

Human dependence upon reliable weather and climate information is increasing. Rainfall is the weather parameter most variable and difficult to measure. Networks of weather radars provide precipitation observations over much of the developed parts of the Earth. However coverage gaps occur even over the continental US, where mountainous terrain obstructs coverage. The lack of flash flood warnings and maritime disaster warnings along the mountainous Pacific coast has cost lives and property loss [1]. The problem is even more acute over developing land and oceanic regions. In order to overcome these limitations and to provide large area coverage, microwave radiometers, such as the SSM/I [2] on the DMSP, the TMI on TRMM [3], the AMSU-A&B on NOAA 15, 16 and 17 and the AMSR-E on AQUA satellites have been placed into low orbits.

http://aqua.nasa.gov

Recently a precipitation radar (PR) on the TRMM satellite has provided high quality, albeit spatially and temporally limited, precipitation measurements over the tropics. Unfortunately temporal gaps in coverage from these low orbiting satellites remain a vexing constraint. The Global Precipitation Mission (GPM) is planned to overcome this limitation by launching many low cost satellites carrying microwave radiometers.

http://gpm.gsfc.nasa.gov

1.1.1 Rain Measurements

Weather radars provide reflectivity measurements over regions whose size is of the order 40,000 km^2 (4×10^6 ha) and they contribute greatly to our understanding of weather in their vicinity [4].

Weather radars are, however, expensive to procure and to operate. They are not found at all in some critical areas — such as the tropics or over oceans. They appear

in insufficient density in mountainous terrain areas. Although satellite observations can provide some continuous information about precipitation, optical techniques are hampered by clouds, and space-borne microwave techniques yield proxy measurements of scattering by icy hydrometeors aloft or the integrated volume emission, with poor spatial resolution and coverage compared to fixed ground instruments.

Rain gauges are very simple, but they provide measurements only at the ground, and no information about the distribution of water and ice above the ground. It would take an uneconomically large number of rain gauges to cover the same area as a single weather radar, so that the simplicity of the individual instrument is overshadowed by the cost and complexity of the data collection network.

1.1.2 Wind Measurements

Tornados [5] produce nature's most violent winds. An average of 800 of these vortices spin up below thunderstorms during a year in the United States alone. Winds in excess of 400 km/hr are generated, potentially devastating entire communities. Doppler radar has proven to be the most significant tornado warning tool in the United States.

Tornados have a characteristic *hook echo* image on radar screens, associated with strong backscatter reflectivities (in excess of 30 dBZ), and strong wind shear. In Fig. 1, we see such an echo. Precipitation reflectivities are indicated on the upper image, with $\sim$5 dBZ intervals showing more rain for red and orange colors, less for the green and blue colors, as evidenced by the scale shown. Note that 29 dBZ is sufficient to identify the *hook* going up the page and then left slightly NW of Newcastle. Wind speed towards and away from the radar are shown in the lower image. The red-tones indicate speed away, green-tones indicate speeds towards the radar, both in 5 m/s intervals.

Hurricanes are a major source of devastation along tropical coastal areas. Anthes [6] cites about 20,000 deaths and more than 7 billion dollars in damage per year around the globe. Hurricanes inflict significant damage through their large scale winds averaging 180 km/hr and gusting to 360 km/hr. Besides damaging houses and harming their occupants, those winds can produce storm surges that inundate coastal cities and destroy ships in coastal waters. Moreover hurricanes may also produce heavy rain, sometimes as much as 100 cm falling within 24 hours. Such rains and concomitant flooding can produce land slides and contaminate drinking water that endanger public health.

The winds of greatest interest to the meteorological community occur within about 150 km of the eye of the hurricane. Rain, of the order 30 mm/hr, is mainly concentrated in 10-20 km wide rain bands that spiral toward the eye as shown in Fig. 2. The radar on board the TRMM satellite shows the Plan Position Indicator distribution of reflectivity (dBZ) and the inserts show the vertical cross sections of reflectivity along

(a) Reflectivity (dBZ) showing Precipitation Rate

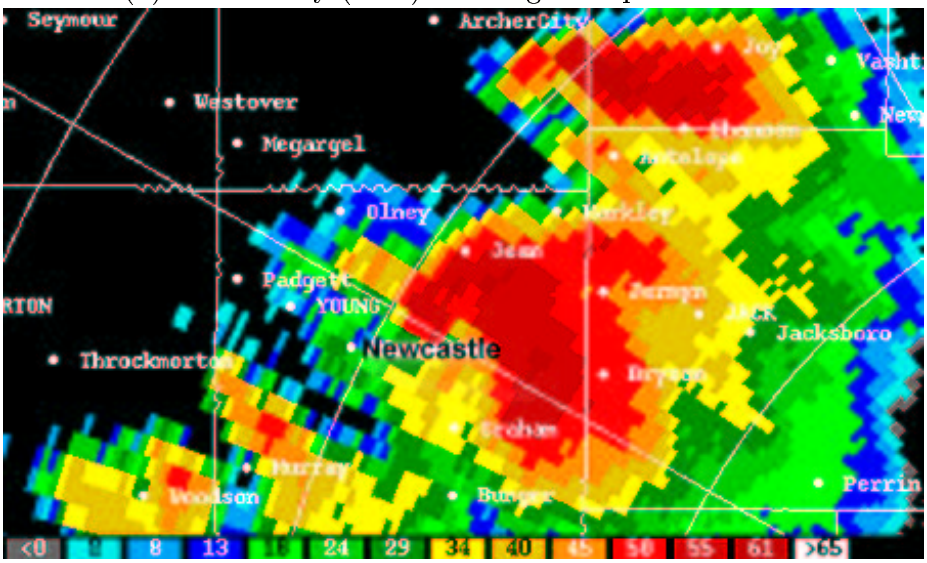

(b) Doppler windspeed (m/s)

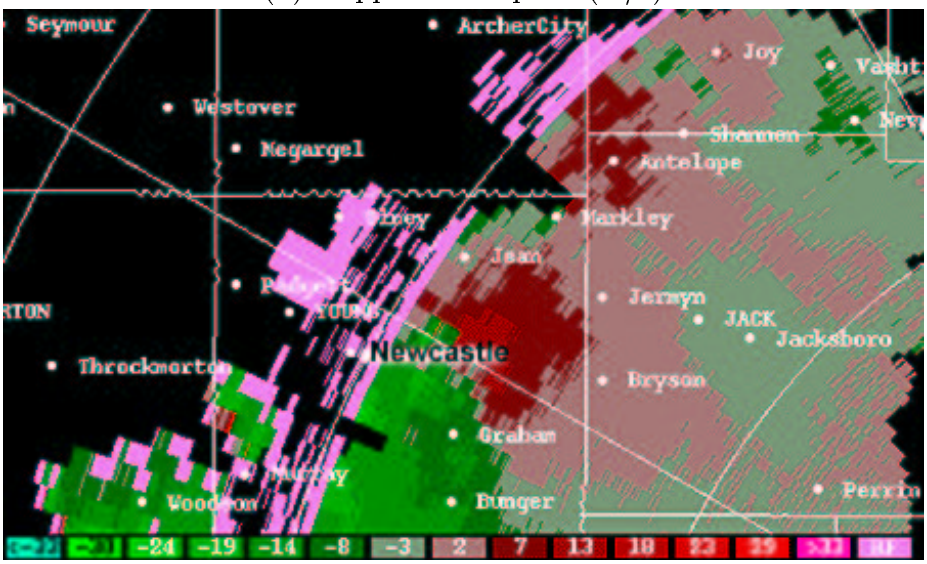

Figure 1: Images captured from existing WSR-88D Doppler radar showing a typical Tornado signature near Newcastle, TX, on 29 May 1995. **These images from the University of Illinois WW2010 Project.** For more information, http://ww2010.atmos.uiuc.edu/(Gh)/guides/rs/rad/appl/trndo.rxml.

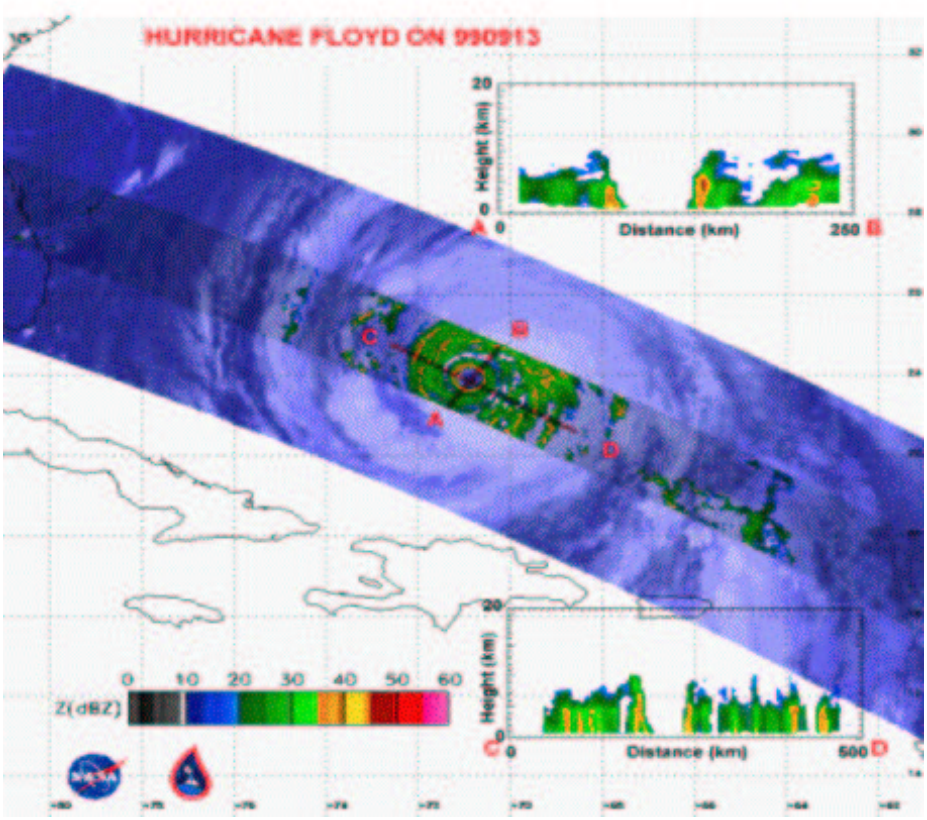

Figure 2: Example of the precipitation reflectivity distribution around Hurricane Floyd on September 13, 1999 observed from the TRMM 14 GHz Precipitation Radar. The larger swath is an infra-red image of the cloud to measured by the Visible Infra-red Radiometric Sensor (VIRS) on TRMM.

the transects A-B and C-D.

The evolution of hurricanes is slow compared to tornados. A PDPR thus can provide adequate measurements at hourly intervals. The winds are also highly organized so that horizontal Doppler measurements at resolution greater than 10 km will suffice for many applications.

1.2 Performance Requirements

The PDPR could be operated in three modes to address various needs. In summary,

- Mode I measures light rainfall (> 17 dBZ), a slowly varying phenomenon. This mode of operation can tolerate higher temporal averaging ($30-60$ minutes) and

larger horizontal spatial resolution blocks (10 x 10 km).

- Mode II measures large-reflectivity returns (> 30 dBZ) like tornados and rapidly variable heavy rainfall. The faster moving phenomenon (typically about 20 km/hr) requires shorter temporal averaging intervals ($5 - 10$ minutes), and smaller horizontal resolution blocks (2.5 x 2.5 km) for effective study.

- Mode III severe weather watch for hurricanes and squall lines, large-reflectivity returns (> 30 dBZ), and moderately variable phenomena that can be monitored with medium temporal averaging intervals ($15 - 30$ min), and larger horizontal spatial resolution blocks (10 x 10 km).

Better performance is desirable, and may be feasible with the forthcoming increase in consumer data bandwidth.

1.2.1 Need for New Measurements

We have begun to investigate a new passive radar technology which provides a data product similar to conventional weather radar, but which is easier and cheaper to deploy and operate. In particular we investigate the possibility of creating a passive weather radar which develops hydrometeor and relative-wind speed information by close observation of the scatter of geosynchronous orbit broadcasts of television and other signals.

Note that reduced cost of a passive Doppler system is conducive to multiple installations, with dual-Doppler measurements admitting computation of horizontal wind velocity rather than the radial wind speed of a conventional active Doppler system. Low cost multistatic, multifrequency observation offers significant immunity to regions with high rainfall and high absorption.

1.3 Passive Radar Development at the University of Washington

We have begun operating a completely passive radar for the observation of ionospheric turbulence [7], the Manastash Ridge Radar (MRR). By carefully observing direct and scattered FM broadcasts at 100 MHz ($\lambda = 3$m), conventional range-Doppler profiles of ionospheric turbulence are created at ranges up to 1100 km. Because the passive system requires no cooperation from the FM broadcasters, all the expense associated with the transmitter is absent. In addition, this passive radar is inherently safe, is completely free of EMI, and consumes little power. Meanwhile, it produces data of unsurpassed quality and sensitivity among ionospheric "coherent" radars.

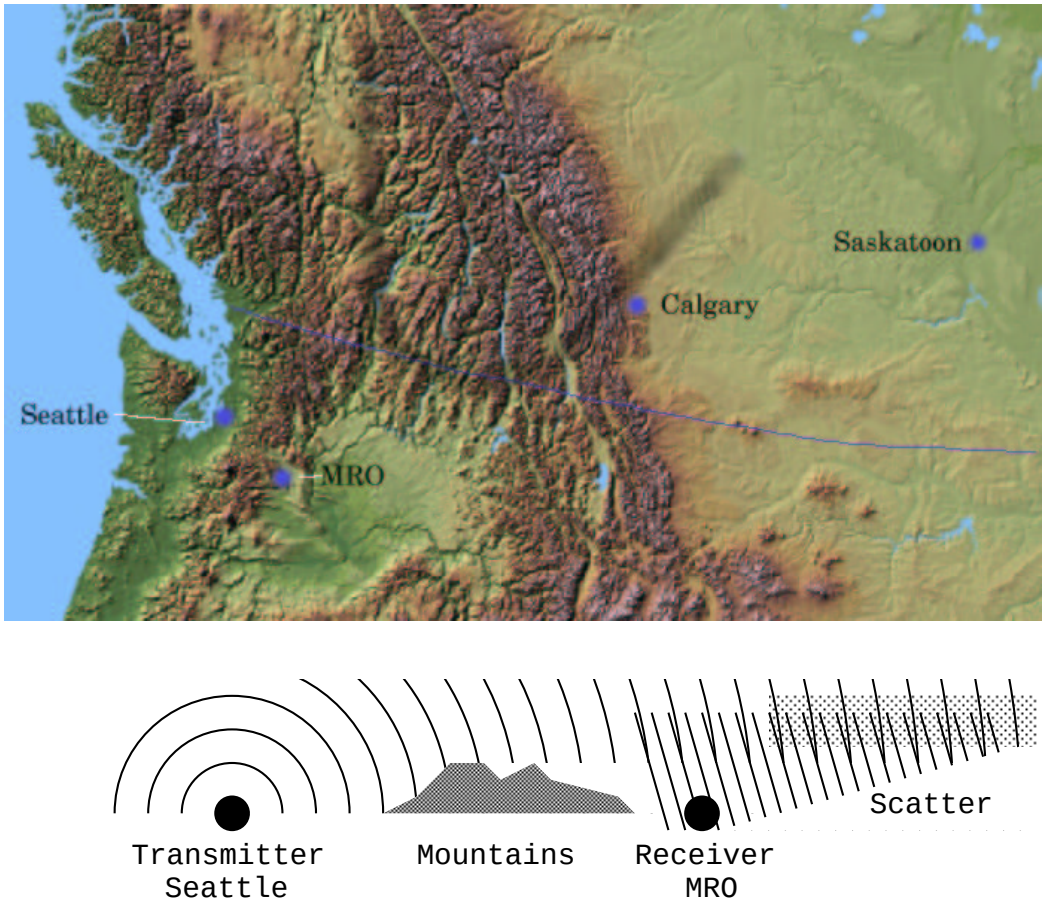

Figure 3: The Manastash Ridge Radar (MRR) is formed by a pair of receivers in Seattle (the reference), and at the Manastash Ridge Observatory (MRO). The MRO receiver is shielded from Seattle-area transmitters by the Cascade Mountains. We plan to place an additional pair of receivers at Calgary and Saskatoon. Although there is no intervening mountain range, these cities lie 600 km apart. (relief map derived from the USGS at `http://nationalatlas.gov/atlasftp.html`)

(a) Quadrantid Meteors, 3 January 2002
vertical: Doppler Velocity, −303 to +303 m/s

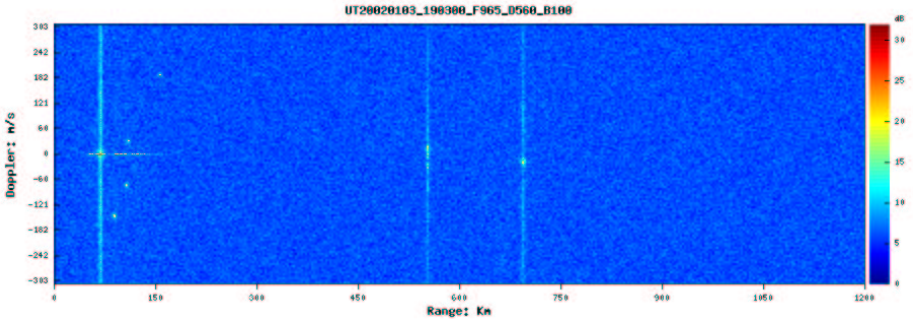

(b) Separated Type 1 echoes, 19 March 2002
vertical: Doppler velocity, −1517 to +1517 m/s

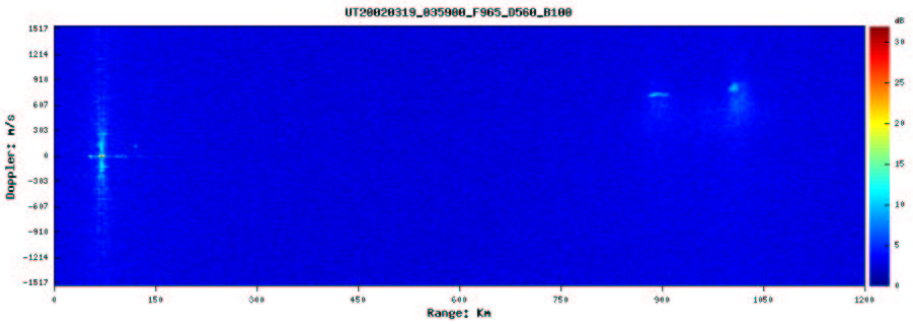

horizontal (a-b): ange, 0 to 1200 km

Figure 4: Two examples of range-Doppler results from the Manastash Ridge Radar at UW. Two meteors (and four aircraft) are shown in the top panel, while the bottom panel shows auroral electrojet echoes during disturbed conditions on 19 March 2002. The common features at a range of 80 km are ground clutter from the Cascades, particularly Mt. Rainier. The radar is in continuous operation, publishing data immediately to the World Wide Web, see **http://www-rcs.ee.washington.edu/∼radar/Data** and **http://www-rcs.ee.washington.edu/rrsl** for more information.

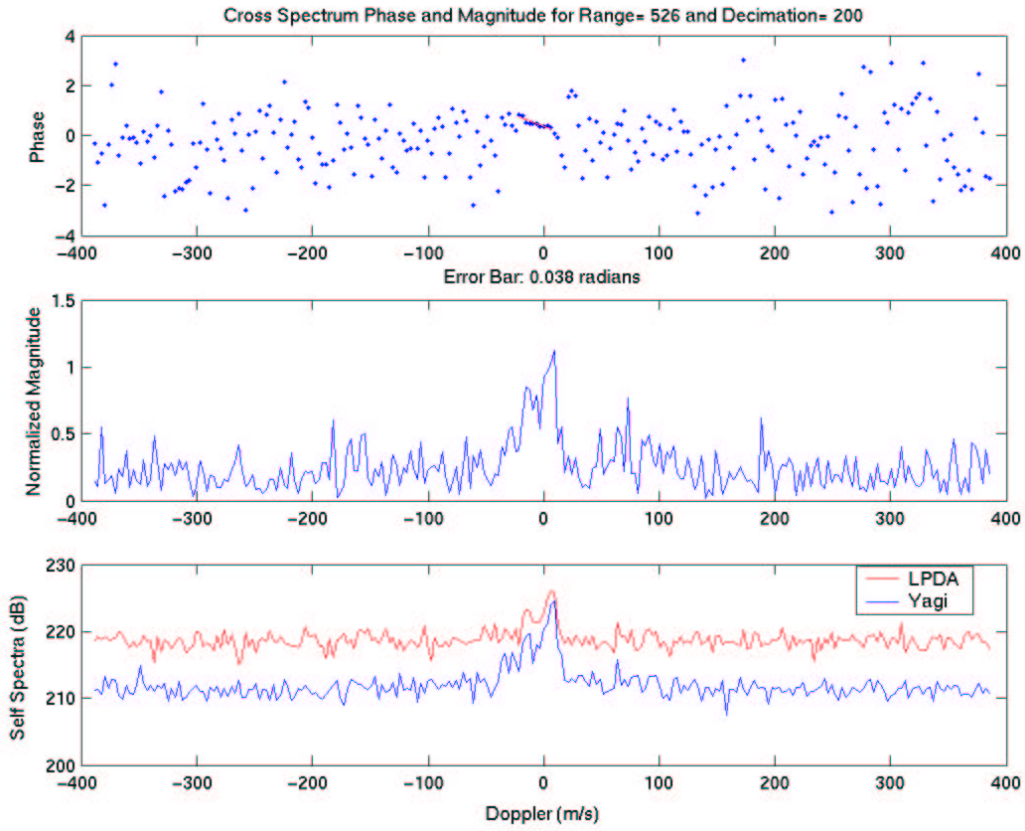

Figure 5: Horizontal interferometric observation of a meteor trail during the January 2002 Quadrantids. The two antennas are separated by 16λ received scatter from the meteor; and the power spectra are shown in the bottom panel. The top panel shows the relative phase between the antennas; the slope reflects the wind shear. Near 0 Doppler velocity, the phase angle is well defined, with high coherence, from which the direction of arrival can be inferred.

Signal processing is correlation FFTs and requires about 5 bops (billion operations per second).

Fundamentally the MRR consists of two receivers and a computational correlation engine. One receiver is located near the transmitter, and provides high quality samples of the original broadcast. The other receiver is located far from the transmitter (beyond a mountain range) and collects the weak scattered signal. The "cross ambiguity function" provides complete range-Doppler profiles of the scatter. Furthermore, we have recently introduced a second antenna and now can perform interferometry to provide angular information about the scatter. In Fig 3 we sketch the MRR system and in Fig 4 and Fig 5 we provide some data examples. Of particular note, the MRR is fully automated and its data may be examined at the World Wide Web site indicated on Fig 4.

The MRR represents the first high performance passive radar for ionospheric applications, however there has been somewhat longer development of passive radar for aerospace applications. In particular Lockheed Martin's "Silent Sentry" represents the greatest achievement [8].

1.4 Passive Weather Radar?

Although VHF wavelengths used by MRR and Lockheed-Martin are far too large for weather radar application, we can nevertheless inquire if different illuminators provide more suitable wavelengths. We must address several fundamental questions before proceeding to a more detailed evaluation.

- **Is there a wavelength-appropriate illuminator?** Weather radars use wavelengths in the range 10 to 3 cm to maximize the Rayleigh scatter while minimizing attenuation. There are numerous geosynchronous orbit transmitters in this frequency range; a few examples appear in Table 1, which includes an example web site of many more.

- **Is the illumination bright enough?** Spacecraft signals are relatively weak at the ground, and the scattering is weaker still. Is there any hope of detecting the weak scatter from such weak sources? Two aspects of the problem drastically improve the likelihood. First, we are not attempting to detect the information encoded in the waveform (whose bandwidth is perhaps 36 MHz), but rather the narrow band signal scattered by precipitation (whose bandwidth is perhaps 200 Hz). As we will see below, the large difference in bandwidth provides sufficient range resolution and large processing gain for SNR improvement.

- **Is receiver algorithm tractable?** Passive radars such as MRR require significantly more computation to extract range-Doppler information than do con-

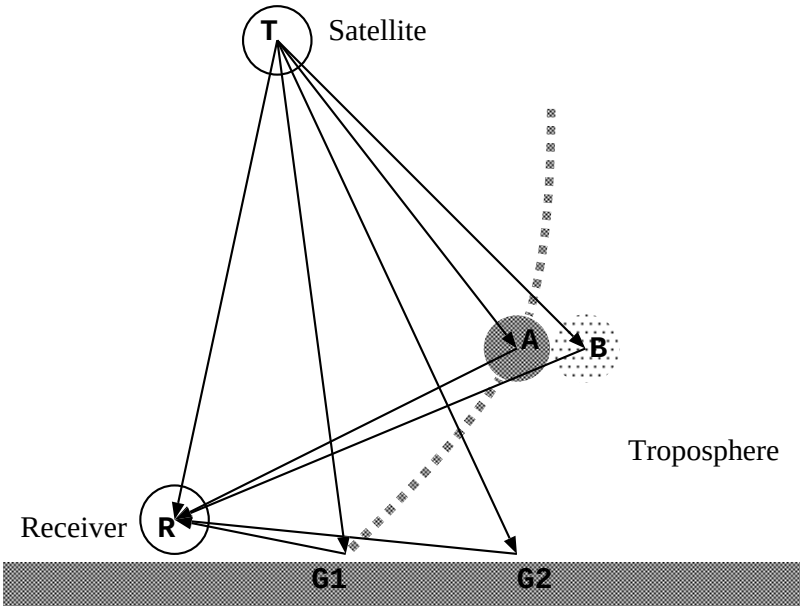

Figure 6: The broadcast satellite orbits about 36,000 km above the Earth, so that rays TR, TA, TB, TG are approximately the same length. For a particular propagation delay, the rain element at A appears, as well as all other points along the dashed line, including the ground clutter at G1; the dashed line is an ellipsoid of constant bistatic propagation delay. There is also rain clutter at different delays (B) and ground clutter at different delays (G2).

ventional radars. We will see that a PDPR has enormous computational requirements; however this challenge has been addressed by radio astronomers, and is accessible with currently available technologies.

1.5 Weather Radar Geometry

In order to understand the discussion which follows, it is critical to be aware of the geometry under consideration, shown in Fig. 6. As in the MRR, true range resolution is developed by fully detecting the scattered waveform against the transmitted waveform, so constant range surfaces are ellipsoids whose foci are the satellite and the receiver. Because the surfaces will be relatively close to the receiver focus, these surfaces are quite close to paraboloids which are highly inclined with respect to the ray RA, as opposed to being normal to the ray for monostatic radars.

Because several different transmitters can be observed, dual and multiple Doppler measurements can be made from a single receiver to provide true vector wind velocities.

Table 1: A few examples of available geosynchronous orbit transmitters. There are a variety of WWW based resources, e.g. `http://www.geo-orbit.org`.

name	frequency	EIRP (dBW)	East long.	illuminates
Hispasat	12 GHz	42	−30	NE Brazil region
Intelsat 709	11-13 GHz	49	−50	Brazil region
Intelsat 805	12.5 GHz	52.7	−55	N Brazil, Colombia, etc
Telstar 6	11-14 GHz	48	−83	Central America
Telstar 6	11-14 GHz	48	−83	Central America
BDS 2/3				Eastern US
Telstar 4	C-band	40	−89	Eastern U
Telstar 4	Ku-band	47	−89	Eastern US
Telstar 7	C-band	39	−129	Western US
Telstar 7	Ku-band	43	−129	Western US
Globalstar	6.875-7.055	30	LEO	
Iridium	19.4-19.6	31.4	LEO	

2 Radar Equation Analysis

For a more quantitative treatment of the statements above, we investigate the radar equation for the active and passive radar cases, deriving both from the more general bistatic radar equation.

$$P_r = \frac{P_t G_t}{4\pi R_t^2} \frac{\sigma V}{4\pi R_r^2} \frac{G_r \lambda^2}{4\pi} \eta \, \xi_r \, \xi_t \tag{1}$$

$P_{t,r}$	received and peak transmitted power, W
$G_{t,r}$	transmit and receive antenna gain, (unitless)
λ	wavelength of selected transmitter, m
R_t	distance from transmitter to scattering volume, m
R_r	distance from receiver to scattering volume, m
σ	volume scattering cross section, m^2/m^3
V	scattering volume m^3
ξ_r	path attenuation to receiver
ξ_t	path attenuation from transmitting satellite
η	efficiency factors (polarization, propagation factors, etc.)

The attenuation factors ξ are related to path integrals of the specific attenuation,

$$\xi = 10^{\left[-\frac{1}{10}\int \alpha(s) ds\right]}$$

recalling that the units of α are dB/km.

The equation above is organized by factors of the transmitted Poynting flux, the scattered Poynting flux, and the receive antenna area. Because the precipitation target fills the antenna beam, the radar equation is commonly written in a somewhat different form for precipitation radar applications[2]:

$$P_r = \frac{\pi^3 P_t G_t G_r \theta^2 c\tau K^2 Z_e}{2^{10} \lambda^2 R_t^2 \log 2} \, \xi_r \, \xi_t \tag{2}$$

$P_{t,r}$	received and peak transmitted power, W
$G_{t,r}$	transmit and receive antenna gain, (unitless)
λ	wavelength of selected transmitter, m
R_t	distance from transmitter to scattering volume, m
θ	receive antenna half-power beamwidth
K	dielectric function $K = (\epsilon - 1)/(\epsilon + 2)$
Z_e	effective reflectivity
$c\tau$	range resolution for a pulse of width τ
ξ_r	path attenuation to receiver
ξ_t	path attenuation from transmitting satellite

This equation can be adjusted further to make comparison between conventional radars (e.g. NEXRAD) and passive systems more apparent. The combination $P_t G_t$

[2]see http://www.osf.noaa.gov/eng/BRFCAL.htm

is the Effective Isotropic Radiated Power (EIRP); also, since $\pi\theta^2$ is the beam solid angle, or $\Omega = 4\pi/G_r$ we have $G_r\pi\theta^2 = 4\pi$; also for monostatic radar systems, $\xi_r = \xi_t$, thus

$$P_r = \frac{\pi^3 P_t G_t c\tau K^2 Z_e}{2^8 \lambda^2 R_t^2 \log 2}\, \xi^2 \tag{3}$$

2.1 Radar Reflectivity, Z_e

The radar reflectivity Z_e deserves special mention. It is the result of analysis of volume Rayleigh scatter, and is defined in such a way as to be wavelength independent, and resolution independent[9]:

$$Z_e = \frac{\sum_n D_n^6}{V} \tag{4}$$

where V is the volume in which a set of drops of diameter D_n appear. It has dimensions of length^6/length^3.

It is common to create a logarithmic scale for Z_e, namely dBZ, for which the reference level dBZ = 0 is defined to be 10^{-18} m^6/m^3, namely the reflectivity of a single, 1 mm diameter drop in a 1 meter cube.

As mentioned above, the dielectric function K describes the polarizability of the scatterer. In the case of liquid water $K = 0.930$ (unitless).

2.2 Bistatic Radar, CW illumination

For bistatic continuous wave (CW) operation, we can appeal to the development above, appropriately reinterpreting the terms when necessary. In Eqn. 3 there is no distinction between R_r and R_t, but there is in the bistatic case. However, by identifying the transmitter EIRP as $P_t G_t$ and assuming that the receive antenna is filled with constantly illuminated scatterers, we can use Eqn. 3 in the same form with only two relatively small corrections.

1. Bistatic Rayleigh scatter will be a little smaller for some polarizations, and unchanged for others. We include this effect into the efficiency η. In general this effect will not be significantly different from unity.

2. The range resolution $c\tau$ will be increased by a factor $\sec(\psi)$, see Fig. 7.

Thus we have

$$P_r = \frac{\pi^3 P_t G_t c\tau \sec(\psi) K^2 Z_e}{2^8 \lambda^2 R_t^2 \log 2} \eta\, \xi_r\, \xi_t \tag{5}$$

For the satellite illuminators, the scattering half angle ψ will typically be smaller than about 45°, so that the factor $\sec\psi$ will not be substantially different from unity.

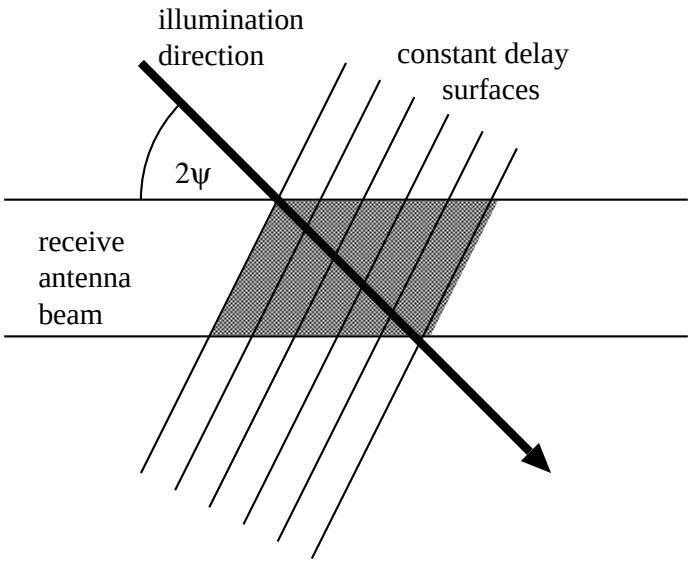

Figure 7: Scattering Geometry. A plane wave (from a satellite not shown in upper left) illuminates a receive antenna pattern (of an antenna not shown left center) at an angle 2ψ (bistatic scattering angle). Planes tilted by the half angle ψ describe surfaces of constant propagation phase delay, so the scattering volume is the tilted, shaded region. Thus the scattering volume is larger by a factor $\sec\psi$. A similar effect modifies the cross track resolution of SAR systems.

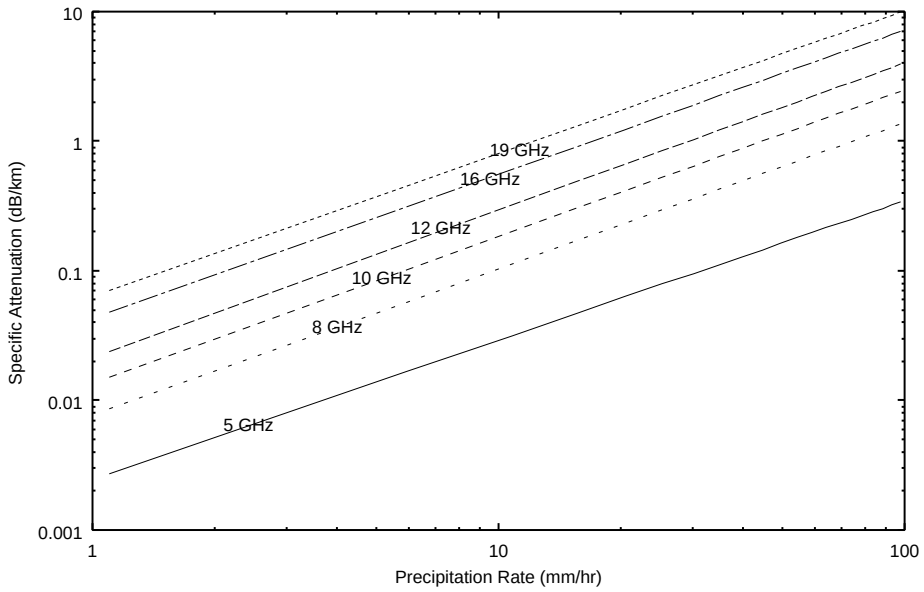

Specific Attenuation, α (dB/km) *vs.* Rain Rate (mm/hr)
for Frequencies of 5,8,10,12,16,19 (GHz)

Figure 8: Several examples of Specific Attenuation as computed per Ippolito [10] for 0 deg rain assuming the Marshall-Palmer distribution. Note that specific attenuation increases nearly linearly with rainrate, and that higher frequencies have higher specific attenuation *vs.* rainrate lines.

2.3 Range independence of Signal

The PDPR has some curious features. Because the illumination source is very distant, the Poynting flux is nearly constant over the entire scattering volume, resulting in very little dependence of the rain signal amplitude on the distance to the receiver. Also, the gain of the receiving antenna does not enter the radar equation (i.e. the *ln 2* factor may be wrong). Note that we can identify Poynting flux $= \frac{P_t G_t}{4\pi (R_t)^2}$ in the radar equation.

2.4 Attenuation

For higher frequencies and higher rain rates, the attenuation along the radar receiving path is of concern. Fig 8 shows specific attenuation *vs.* rainrate for a few frequencies.

Ippolito[10], and references therein describe a good match for measured specific attenuation (dB/km) by

$$\alpha = a\, R^b \tag{6}$$

where a, b are temperature and frequency dependent coefficients and R is the precipitation rate (mm/hr). This approximation has been shown to agree well with Mie scattering calculations of specific attenuation.

2.5 Clutter

We also need to account for the ground clutter. The formulas for this are similar, except that σ^A, the radar cross-section (RCS) per unit area of ground surface, has units of area per area. This is sometimes written as $dBsm/m^2$.

The clutter scattered power at the receiver is a function of the power incident on the unit area of ground surface, diminished by the projected area at the receiver, and falls off with ${R_c}^2$, the distance from the clutter to the receiving antenna. Both the projected area factor and the R_c factor mean that the near-to-antenna ground region dominates the clutter power.

Recall that in Eqn 2, using Eqn 4, the precipitation RCS per volume of rain is

$$\sigma^V = \frac{\sum_j \frac{\pi^5 D_j^6 |K|^2}{\lambda^4}}{\text{volume}} \tag{7}$$

i.e., the sum of the scattering from each scatterer in the volume divided by the volume. For clutter cross-section, we use an empirical value [11] of -10 dB/m^2 for σ^A in an urban terrain, and integrate the contributions to the antenna power received from all illuminated ground area within the antenna field of view.

2.6 Signal Processing

If we directly compare the illumination strength of WSR-88D and satellites, it is not surprising to see that WSR-88D transmitter is far brighter than satellites. However, the peak brightness, or instantaneous signal to noise ratio, does not describe the performance. Consider that NEXRAD operates with a duty cycle of about 0.1 percent, which decreases the average power by 30 dB. Also, NEXRAD scans in azimuth and elevation, with a typical azimuth scan rate of about 20 degrees per second and 14 elevation angle scans, so that a volume scan requires about five minutes. This scan rate means that the antenna slews through about twenty beam widths per second, illuminating a particular scattering volume for only about 50 ms for each 5 minutes (300 seconds). Thus the dwell duty cycle is about 1/6000, another 37 dB loss. For NEXRAD, the average transmitter power illuminating a particular volume is then

$$105\ dBW - 30\ dB - 37\ dB = 38\ dBW.$$

Meanwhile, the satellite illuminates the entire target with 100 percent duty cycle.

The data/communication satellites which PDPR could choose from as sources all have modern modulation schemes which are bandwidth efficient ("noise like"), and

thus have good ambiguity. We expect the consumer demand for higher bandwidth in hand-held wireless data systems will continue to generate brighter sources. Sources exist today to demonstrate the principles.

The detectability also depends upon the noise entering the system. For NEXRAD, the receiver bandwidths must be approximately 1 MHz to accept the transmitter energy. On the other hand, the passive radar processing algorithm permits synthesis of a receiver whose effective bandwidth is quite small, a few hundred hertz, despite the frontend bandwidth of about 30 MHz. For NEXRAD at 500 kHz, averaging 50 pulses yields 10 kHz, compared to PDPR at 36 MHz, but coherent process for 0.1 sec yields 10 Hz. This is yet another 30 dB noise power advantage for PDPR.

The inherent range resolution of the PDPR is very high, 30 MHz corresponding to about 10 m, which is much finer than is needed and provided by WSR-88D, thus the scatter from many ranges can be added (average) to mimic NEXRAD. Therefore such averaging will provide about 10 dB of improvement in SNR through incoherent averaging. Similarly, NEXRAD for 1 km block integration over the 300 m nominal resolution, gains about 2.6 dB in SNR from incoherent averaging.

The principal problem facing PDPR is the large distance from the transmitter, which significantly reduces the poynting flux density on the target. For NEXRAD, this is about 50 km, while for a GEO satellite, this is about 36000 km. That corresponds to a $(50/36000)^2 = -57\ dB$ penalty.

Perhaps the best way to describe the performance of a passive system is to do a direct comparison with NEXRAD, outlined in Table 2. The table compares to the NEXRAD 300 m range resolution, 5 min observation time, and 50 km range.

The data in tables 2 and 3 show that, for 5 minute time resolution, WSR-88 outperforms a passive system by 56 dB in terms of sensitivity for the same size scattering volume and similar size antenna, with NEXRAD reference to 50 km range (the passive system's sensitivity is not dependent upon range). Note that the evaluation of the NEXRAD performance is in line with published specifications[3] which serves as a "sanity check" for table 2. Table 3 contains general capabilities and costs[4] for comparison.

2.6.1 Short Description of Signal Processing

In order to extract the hydrometeor scatter, we need access to two receiver sample streams, the direct path and the scattered path (see Fig. 6). These two data streams must be sampled at the Nyquist rate, yielding a pair of in-phase and quadrature signals $x(t)$ (scatter) and $u(t)$ reference; the Nyquist Rate is approximately

[3] `http://www.roc.noaa.gov/eng/nexradtech.asp`

[4] 1.91± factor of two, see **http://www.eecradar.com**, assumes 50 km range for WSR-88D and 100 km range for PDPR

Table 2: Table comparing radar equation signal powers for active and passive radars. Assume 5 minutes of observation, and identical cross beam antenna patterns (i.e. NEXRAD antenna gain performance). The NEXRAD performance is stated for R = 50 km; the passive radar sensitivity is not dependent upon range to receiver.

	WSR-88D		PDPR	
wavelength	10 cm	20 dB	2.5 cm	32 dB
EIRP P_tG_t		105 dBW		50 dBW
R_t	50 km	-94 dB	36000 km	-151 dB
$K^2\pi^3/(2^8\log(2))$		-8.2 dB		-8.2 dB
$c\tau$	300 m	25 dB	10 m	10 dB
antenna subtotal		47.8 dB		-67.2 dB
coherent integration	1	0 dB	10^5	50 dB
incoherent integration	30	7.5 dB	10^5	25 dB
range average	1	0 dB	30	7.5 dB
integration subtotal		7.5 dB		82.5 dB
subtotal		55.3 dB		15.3 dB
0 dBZ reference		-180 dB		-180 dB
k_BTB		143 dB		126.5 dB
SNR/dBZ		18.3 dB		-38.2 dB

Table 3: Table comparing general capabilities and costs of radars

	WSR-88	PDPR	WSR-57
Doppler	yes	yes	no
polarimetric	no	yes	no
beamwidth	1°	all sky	2°
purchase \$/hectare	1.91	0.06	*obsolete*
operation ¢/hectare/yr	78.2	0.06	*obsolete*

36 Msamp/sec for TV satellite.

The inherent range resolution of these nearly-white signals is found from the correlation time, which is about one baud, or 1/36 MHz = 30 ns, which correspondes to about 5 m. To examine a 100 km range raster, there are therefor 100 km/5 m = 20k ranges. Therefore, the amount of computation associated with developing the range specific correlations is 20k * 36 MHz = 720 B complex multiply/add operations per second per scattering antenna. For a volume scanning interferometric system of N (perhaps 20) antennas, this is approximately 20 T complex multiply/add operations per second, or a total of about 100 T multiply/add operations per second associated with the initial range detection.

The correlator will produce correlations at the target bandwidth rate, about 400 Hz (times 20k ranges). At this point the calculations can proceed in several different ways. For FFT-based Doppler processing, it will be necessary to perform 20k ranges * N antennas * FFT work/s. With 16 pt FFTs, this is 25 FFTs/s/range, or a total of 500k FFTs/sec. Each complex FFT requires 16 log_2 16 work = 64 complex mult/add (about 200 operations), so the FFTs require about 100 M operations per antenna. For 20 antennas, that works out to about 2 B operations per second. These FFTs are multiplied, accumulated, and range-integrated to yield an N by N by 16 real matrix at 100 ranges, this matrix containing the Doppler and interferometric angle information, and being updated at the rate of the integration time (e.g. five minutes).

Note that 2 Bops is quite achievable, and is significantly less than the initial 100 T ops for detection. This is a typical result for a passive radar system; that the lion's share of computation lies in the initial detection, and that the subsequent processing is small in comparison. Although the init operations count is large, these are simple add-multiply operations that can be easily integrated into VLSI — and have been already been used[12], by radio astronomers in support of VLBI, which contains an essentially identical operation.

Thus, for an operational system the net computational burden is about 100 Tops. For a real-time capable demonstration, with a single antenna and a restriced range, the computational burden is about 1 Top, and a non-real-time demonstration system could work with about 50-100 Gops, processing data after strong rain events only.

2.7 Signal to direct path ratio

We also need to account for the receiver competition between the direct and scattered paths. With the Friis Transmission formula [13] we have

$$P_d = \frac{P_t G_t}{4\pi R_t^2} \frac{G_r' \lambda^2}{4\pi} \tag{8}$$

If we compute the scattered to direct power ratio, many terms cancel, leaving

$$\frac{P_r}{P_d} = \frac{\sigma}{4\pi R_r^2} \frac{G_r}{G_r'} \tag{9}$$

In terms of radar reflectivity, we have

$$\sigma = \frac{\pi^5 K^2}{\lambda^4} ZV \tag{10}$$

and

$$V = c\tau R_r^2 \frac{4\pi}{G_r} \tag{11}$$

Thus

$$\frac{P_r}{P_d} = \frac{\pi^5 K^2 Z c\tau R_r^2 4\pi}{G_r \lambda^4 4\pi R_r^2} \frac{G_r}{G_r'} = \frac{\pi^5 K^2 Z c\tau}{G_r \lambda^4} \frac{G_r}{G_r'} \tag{12}$$

At Ku band ($\lambda = 2.5$ cm), with $G_r = 47$ dB, and $G_r/G_r' = 30$ dB, we have

$$\frac{P_r}{P_d} = 1.35 \times 10^5 Z \frac{G_r}{G_r'} \tag{13}$$

where G_r/G_r' is simply the relative antenna response in the scatter direction versus the path to the satellite (the sidelobe level). We suggest that 30 dB ought to be fairly easy to achieve.

If we expect to be able to detect reflectivity of +30 dBZ, this implies a Z = 10^{-15}, so that $P_r/P_d = -62$ dB. In other words, the scattered signal will be very small compared to the direct path illumination — which we expect. However, we have two signal processing cards to play.

1. "Sidelobe cancellation" The direct path signal will be accurately measured and can be coherently subtracted from the scatter paths; currently technology makes 20 dB readily accessible.

2. The scattered signals will arise from ranges at significant delay, which means that the signal processor will coherently reject the direct path. Since the coherent integration time lasts for about 10^5 samples, we gain 50 dB of improvement here.

Thus standard signal processing tools will provide about 70 dB of additional rejection of the direct path jamming, permitting the detection of targets brighter than 30 dBZ.

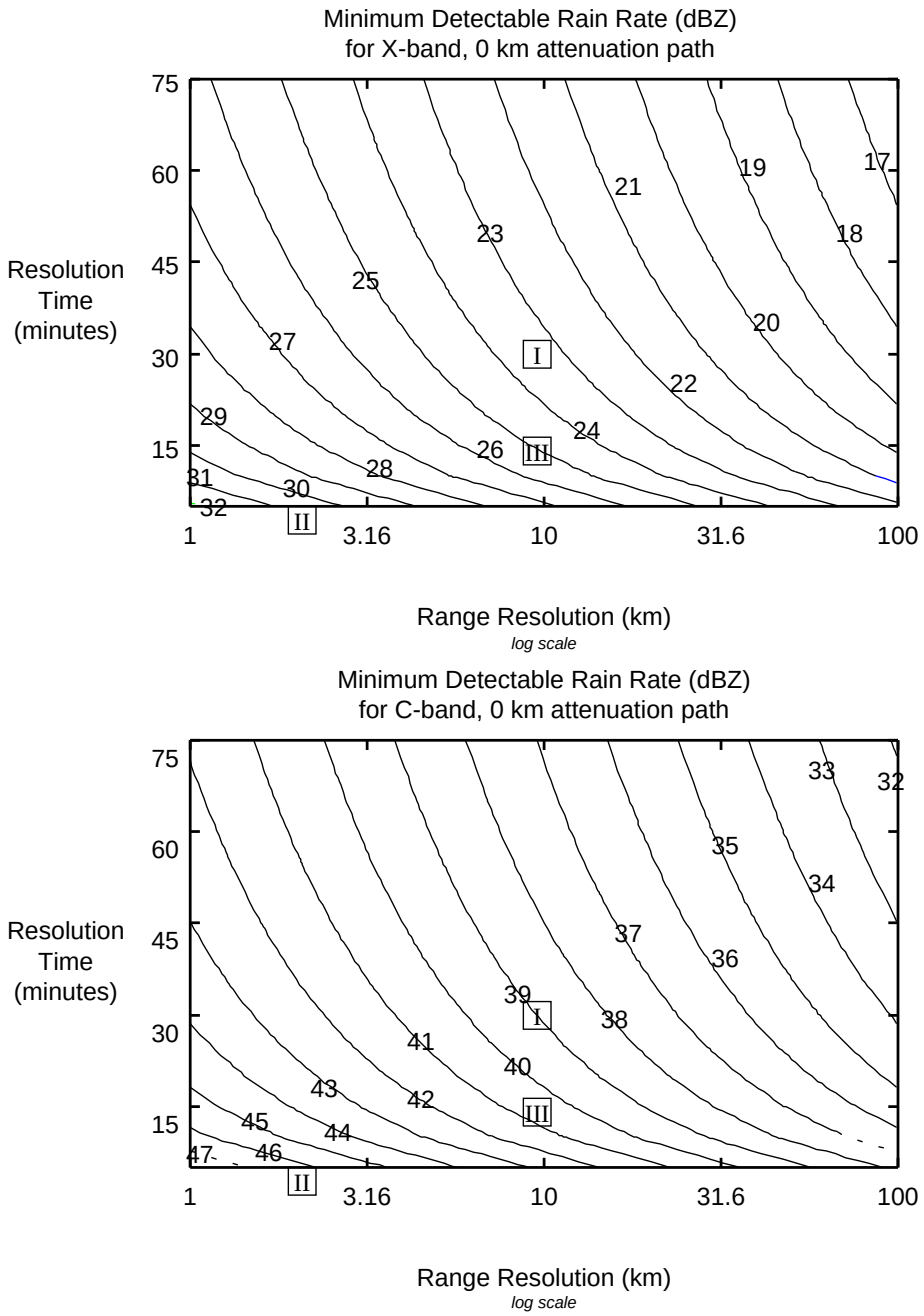

(a) X-band, (b) C-band

Figure 9: Effect of range-averaging and time-averaging of the PDPR data is shown for C-band (39 dBW EIRP) and X-band (50 dBW EIRP) examples, for a 0 km attenuation path. The X-band case shown in (a) appears in Table 2. The location of the three performance modes are indicated with boxed symbols I, II, III.

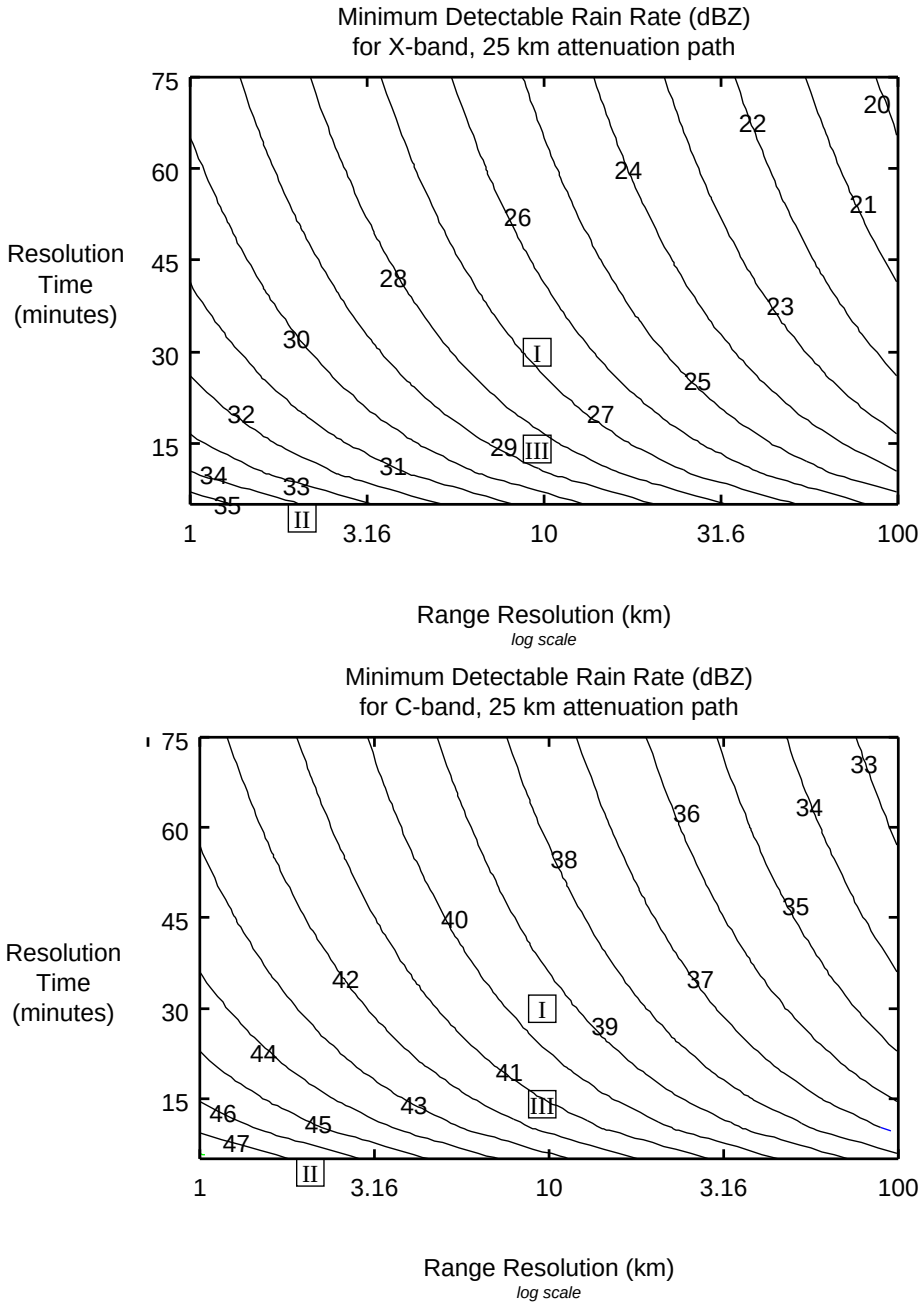

(a) X-band, (b) C-band

Figure 10: Effect of range-averaging and time-averaging of the PDPR data is shown for C-band (39 dBW EIRP) and X-band (50 dBW EIRP) examples, for a 25 km attenuation path. The location of the three performance modes are indicated with boxed symbols I, II, III.

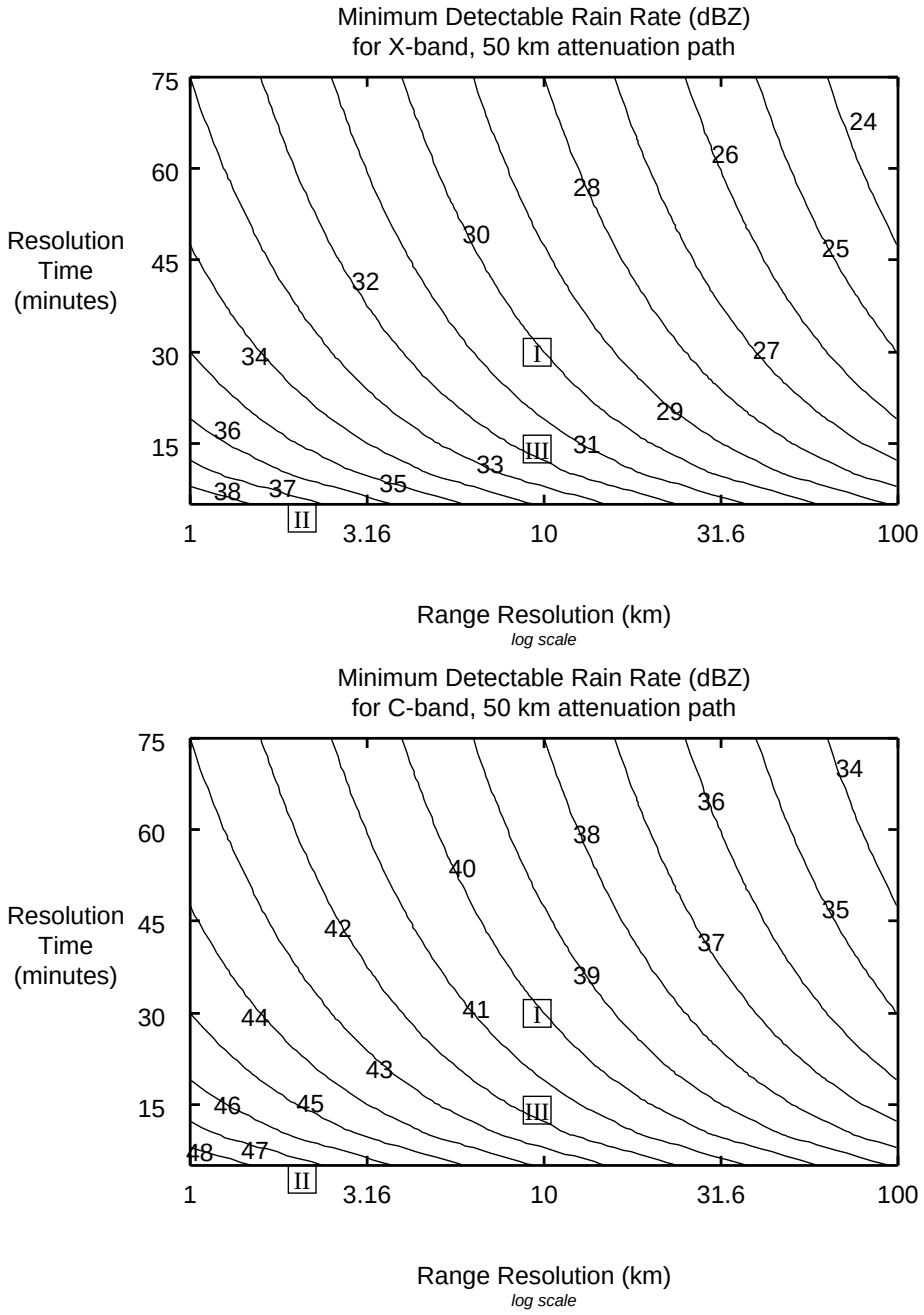

(a) X-band, (b) C-band

Figure 11: Effect of range-averaging and time-averaging of the PDPR data is shown for C-band (39 dBW EIRP) and X-band (50 dBW EIRP) examples, for a 50 km attenuation path. The location of the three performance modes are indicated with boxed symbols I, II, III.

2.8 Summary of Analysis

Estimated sensitivity versus range and integration time are depicted in Figures 9, 10, and 11. In each of these figures, the three performance modes have been located with boxed symbols I, II, III.

Current capability of PDPR is about 35 dBZ which corresponds to a rain rate of approximately 5.5 mm/hr which may be useful for weather avoidance for aviation, and for tornado watchers, taking advantage of the readily available Doppler information. Clearly greater sensitivity, e.g. 17 dBZ, would have more applications.

3 Prototype Implementation Future work recommendations

With such mild success, it needs to be stated that the Proof of Concept could be achieved with current technology for ten to twenty thousand dollars in hardware, assuming $G_r = 30$, $\lambda = 3$ cm. The low-altitude, high-precipitation detection could be of use to the aviation community today. And, hand-held wireless data services are coming, so enhanced sensitivity is on its way.

3.1 Initial Ground-based test

Proof of concept could be constructed with a fixed ground-based antenna pair. One points full-time to the GEO satellite source selected. The second points full time at a solid angle of space which rain can be expected to fall through. Receiver and processor hardware complete the major items in such a system.

Significant engineering challengs must be addressed to create a full implementation of the PDPR. Many of the issues can be well illuminated with a relatively simple and inexpensive system consisting of two identical high gain antennas, illustrated in Fig 12. One antenna is pointed at the illuminating satellite to provide the reference signal; a second antenna is pointed to collect scatter from rain events. It will be useful if the second antenna is pointed in a direction which minimizes direct path from the satellite.

These two antennas would then be connected to synchronous digital receivers in exactly the same fashion as the MRR system, and the usual correlation process would be applied to the resulting data. If a third antenna were used, it would be possible to investigate interferometric operation.

Following successful ground based proof of concept, additional analysis would be needed to complete the design.

Use of interferometry to take advantage of all-angle information would be efficient.

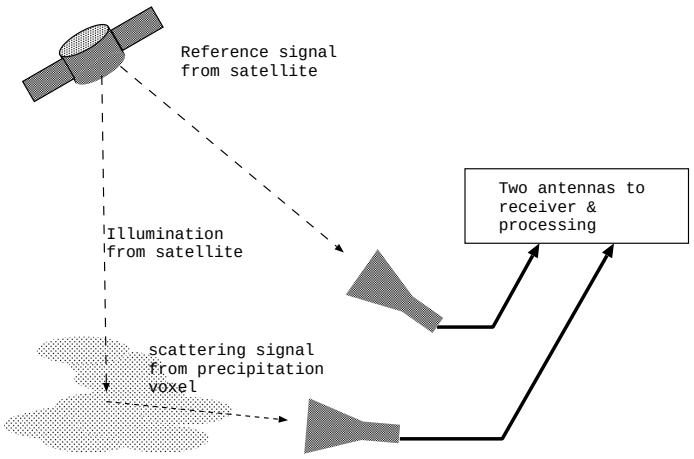

Figure 12: Rough sketch of proof-of-concept system, comprised of two fixed antennas, one targeting a GEO source satellite, one targeting a voxel of space in which we seek the precipitation rate.

There are three general techniques for achieving resolution in azimuth and elevation. WSR-88D and predecessor radars all scan a single high gain antenna to build up the information over several minutes. Another possibility would be to use a phased array; to achieve the spatial resolution of NEXRAD would require thousands of antenna elements, which for PDPR would generate a truly frightening computational burden.

The remaining technique is interferometric imaging, which is well-suited to the broad illumination provided by the satellites. Radio astronomers have developed extremely sophisticated implementations of this concept, which includes mitigation of interference. One difference is that the radio astronomy field of view is fairly small, with thousands of baselines, compared to the nearly hemispherical view of a PDPR, with about 20 antennas and about 200 baselines.

Suppose that, at a particular range, the scattering cross section is distributed as $I(\Omega)$, and that there are N antennas with gains $g_n(\Omega)$. Then the pairwise correlations R_{nm} can be shown to be Fourier-like transforms of I, namely

$$R_{nm} = \int g_n(\Omega) g_m^*(\Omega) \exp(jk\hat{\Omega} \cdot *(\vec{x}_n - \vec{x}_m)) I(\Omega)\ d\Omega \tag{14}$$

It is possible to additionally index $R(\nu)$ to capture the spatial Doppler distribution. A variety of methods for inversion of R_{nm} are available; the broad spatial distribution of rain suggests that the Maximum Entropy Method or variations would be a good choice. MEM is able to generate high resolution where SNR is large, permitting the precise location of bright scatterers.

Although development of this algorithm would be needed, the problem is fairly well posed, and considerable experience is available from the radio astronomy community.

4 Interpretation and Summary

The performance estimates in Table 2 show that the baseline sensitivity of a passive system is far less than that of an active system. This low performance arises from low EIRP and very large distance to the transmitter, namely the very low Poynting flux on the target.

Although a significant portion of the deficit can recovered by signal processing, a significant performance deficit remains. Despite this marginal performance, some interesting opportunities remain.

Because the poor sensitivity of the envisioned PDPR will be of little use in regions with light rainfall, it nevertheless can be be of use in regions with heavy rainfall. Such regions are found near hurricanes in the tropics as well as in frontal systems at higher latitudes. Because the PDPR has potentially very fine range resolution and full Doppler spectrum estimation, it could be of some use in studying severe storms with heavy rain, hail, and high winds.

Although the computational challenges are large, the fundamental limitations are associated with weak illumination. The PDPR could certainly be used to extend conventional radars by providing additional bistatic receivers (without requiring heavy coordination with the existing transmitters). This would provide opportunities for "gap filling" when existing weather radars have marginal performance because of large ranges or terrain limitations.

Although the PDPR is envisioned as a completely passive, noncooperative system, there is no reason that it could not be co-developed with dedicated sources. A higher power-aperture product (70 dBW as opposed to 50 dbW) would immediately provide 20 dB greater sensitivity. Thus, a few satellites could provide bright illumination of regions which had been seeded with PDPR receivers. Certain waveform choices would relieve the signal processing problem substantially, while preserving the basic CW system.

Also, PDPR provides an alternate design paradigm for conventional weather radars. As a rainfall surveillance system the system performance is limited not by the power aperture product (105 dB for WSR-88D), but instead by the average transmitter power — which is effectively 38 dBW (6.5 kW). Rather than building a high performance reflector and mechanically steering it, a vastly simpler system would employ omnidirectional CW illumination from a very small, rigid antenna, supported by PDPR-like receivers in the vicinity. Furthermore, it might be possible to use higher frequencies, which would permit the reduction of the transmitter power further (be-

cause of enhanced scattering cross section). It is quite possible to imagine providing coverage equivalent to current WSR-88D installations with a few omnidirectional microwave broadcasts of about 1 kW, of vastly simpler structure than the WSR-88D. In essence, the part of the radar performance provided by high peak power and large reflector area is accounted for by moderate average power, simple antennas — and very large computation. From a technological point of view, only computational power is becoming cheaper; there is no reason to expect that high power microwave transmitters and large parabolic dishes with radomes will become inexpensive.

Our investigation of PDPR thus suggests that the PDPR as conceived would have marginal performance. However, at the same time there are a variety of interesting variations on the theme which may well provide very high performance at very low cost. As in the case of the ionospheric radars which inspired this project, the key is to reduce emphasis on technologies whose performance to price ratio is static (high peak power, large antennas), and increase emphasis upon technologies performance to price ratio is very rapidly improving. The amount of computation required for systems like PDPR is very large, but the cost of that computation is plummeting, and the results should be just as large.

In summary we look forward to the development of high performance, low cost, computation-centric radar systems for many remote sensing applications.

Index

References

[1] K.J. Westrick, C.F. Mass, and B.A. Colle. The limitation of the WSR-88D radar network for quantitative precipitation measurements over coastal western united states. *Bull. Am. Met. Soc.*, 80(0):2289–2298, 1999.

[2] J. Hollinger, J. Pierce, and G.A. Poe. SSM/I instrument evaluation. *IEEE Trans. Geosci and rem. Sens.*, 28(0):781–790, 1990.

[3] C. Kummerow, W. Barnes, T. Kozu, J. Shiue, and J. Simpson. The tropical rainfall measuring mission (TRMM) sensor package. *J. Atm. and Ocean. Tech.*, 15(0):808–816, 1998.

[4] Richard J. Doviak. *Doppler Radar and Weather Observations.* Academic, 1984.

[5] William L. Donn. *Meteorology.* McGraw-Hill, NYC, 4 edition, 1975.

[6] R.A. Anthes. *Tropical cyclones, Their evolution, structure and effects.* American Meteorological Society, Boston, MA, 1982.

[7] J. D. Sahr and F. D. Lind. The Manastash Ridge Radar: A passive bistatic radar for upper atmospheric radio science. *Radio Sci.*, 32:2345–2358, 1997.

[8] David A. Fulghum. Space tracking plan eyes mobile missiles. *Aviation Week and Space Technology*, 18 Jan 98:61 ff, 1998.

[9] L.J. Battan. *Radar Observation of the Atmosphere.* Univ. of Chicago Press, Chicago, 1973.

[10] Louis J. Ippolito. *Radiowave propagation in satellite communications.* Van Nostrand Reinhold, New York, 1986. ISBN 0-442-24011-2.

[11] M. I. Skolnik. *Radar Handbook.* McGraw-Hill, New York, 3rd edition, 2001.

[12] James M. Moran George W. Swenson Jr Thompson, A. Richard. *Interferometry and Synthesis in Radio Astronomy.* John Wiley and Sons, NYC, 2 edition, 2001.

[13] Robert E. Collin. *Antennas and Radiowave Propagation.* McGraw–Hill, 1985.